nature nanotechnology

Letter

https://doi.org/10.1038/s41565-022-01252-8

Giant bulk piezophotovoltaic effect in 3R-MoS_2

In the format provided by the authors and unedited

1. Theoretical model for strained 3R-MoS_2

We perform a theoretical calculation of linear and nonlinear conductivities in the strained 3R-MoS_2. To this end, we consider a tight-binding model for MoS_2 based on Ref.[S1] as follows. MoS_2 consists of Mo and S, where p_x, p_y, p_z orbitals of S and $d_{z^2}, d_{xy}, d_{x^2-y^2}$ orbitals of Mo play important roles to describe the electronic structure around the Fermi energy. Thus, we considered a model for a single layer consisting of these six orbitals connected through nearest neighbor couplings and next nearest neighbor couplings between different sublattices as a building block. In order to construct the model for 3R-MoS_2, we incorporate an interlayer coupling V between p orbitals of S atom in the neighboring layers as given in Eq. 16 in Ref. [S1]. As a consequence, the tight-binding model for 3R-MoS_2 ($H_{3\mathrm{R-MoS_2}}$) takes the form

$$H_{3\mathrm{R-MoS_2}} = \begin{pmatrix} H_{\mathrm{MoS_2}} & V & V^\dagger \\ V^\dagger & H_{\mathrm{MoS_2}} & V \\ V & V^\dagger & H_{\mathrm{MoS_2}} \end{pmatrix}.$$

where $H_{\mathrm{MoS_2}}$ is the Hamiltonian of a single layer MoS_2 and we adopted orbitals labeled from 6 to 11 in Table II of Ref. [S1], and used the hopping parameter in Table VII in Ref. [S1]. For simplicity, we neglected the coupling to other orbitals (labeled from 1 to 5), because it is weak compared with the energy splitting between 1 to 5 and 6 to 11 orbitals. We constructed the interlayer coupling V from Eq. 16 in Ref. [S1], using distances between atoms that are listed in Table I of Ref.[S1]. We introduced the strain effect to the above model by two phenomenological parameters ε_x and ε_y that uniformly modulate hopping amplitudes in the x and y directions. When we apply the strain to the y-direction, distance between two sites becomes longer along the y-direction and shorter along the x-direction. Since the hopping amplitude depends on the distance between two sites, the hopping amplitude along the x-direction increases and decreases along the y-direction. In this model, we take the armchair direction to the y-direction, and modulated hopping amplitudes in the way depicted in Supplementary Fig. 1a, b, which assumes a simple power form with respect to the parameters ε_x and ε_y according to the hopping distance. In the numerical calculations, we set $\varepsilon_x = 1.1$ and $\varepsilon_y = 0.9$. The band structure calculated based on this model is presented in Supplementary Fig. 1c, showing a bandgap of 1.5 eV at K and K' points that is highly consistent with the value in previous work[S3].

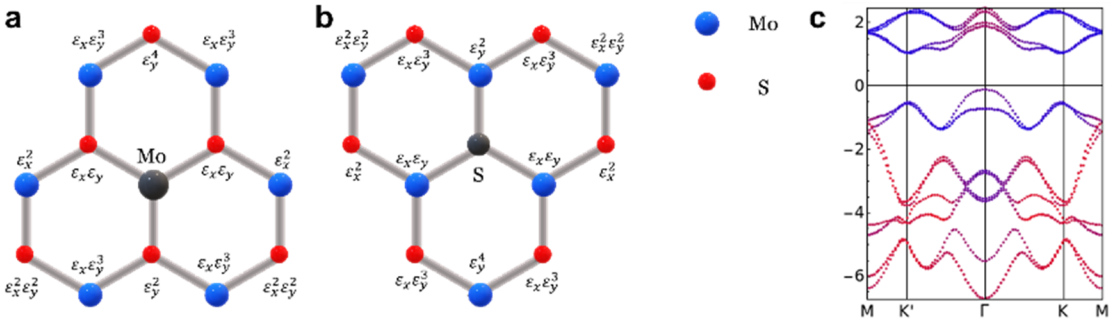

Supplementary Fig. 1| Phenomenological modulation of hopping amplitudes for the strained systems. a,b, Modulation factors of hopping amplitudes for the strained systems. Hopping amplitudes between the center atom (depicted by a black circle) and other atoms are multiplied by modulation factors shown near the atoms, which gives a phenomenological modeling of the strain effect. Blue circles represent Mo atoms and red circles represent S atoms. **a,** The case when the center atom is Mo. **b,** The case when the center atom is S. **c**, The band structure of the tight-binding model for strained 3R-MoS_2. Here, the red and blue color indicate the contribution of p-orbitals and d-orbitals.

2. Calculation of photovoltaic coefficient β and its strain dependence

Photocurrent along the a-direction J_a induced by the electric field of linearly polarized light along the b-direction E^b is described by the coefficient β_{ab} as

$$J_a = \frac{\epsilon_0 c}{2}\beta_{ab}E^b(\omega)E^b(-\omega).$$

Here, ϵ_0 is the vacuum permittivity, c is the speed of light. To compute this coefficient, we used the formula in Ref.[S2],

$$\beta_{ab} = \frac{4\pi g_s e^3}{\hbar^3 \epsilon_0 c}\sum_{nm}\int \frac{d^2k}{(2\pi)^2}\, f_{nm} I_{nm}^{abb}\ \delta(\omega_{nm}(\boldsymbol{k}) - \omega),$$

with $f_{nm} = f_n - f_m$ and $\omega_{mn} = E_m - E_n$. Here, f_n and E_n are the Fermi distribution function and the energy eigenvalue for the band n. g_s is the spin degeneracy, I_{nm}^{abb} is defined as $I_{nm}^{abb} = \mathrm{Im}\left(\mathrm{r}_{mn}^b r_{nm;a}^b\right)$. r_{mn}^a is expressed as $\mathrm{r}_{mn}^a = iv_{mn}^a/\omega_{mn}$ and

$$r_{nm;a}^b = -\frac{1}{i\omega_{nm}}\left[\frac{v_{nm}^a\Delta_{nm}^b + v_{nm}^b\Delta_{nm}^a}{\omega_{nm}} - w_{nm}^{ab} + \sum_{p\neq n,m}\left(\frac{v_{np}^a v_{pm}^b}{\omega_{pm}} - \frac{v_{np}^b v_{pm}^a}{\omega_{np}}\right)\right].$$

Here, v_{nm}^a is the velocity matrix element for the velocity operator along the a-direction given by $v_{nm}^a = \langle n|\, \partial_{k_a} H(k)|m\rangle$ with the eigenvector $|n\rangle$ for the band n. $\Delta_{nm}^a = v_{nn}^a - v_{mm}^a$ and $w_{nm}^{ab} = \langle n|\, \partial_{k_a}\partial_{k_b} H(k)|m\rangle$. In numerical calculations, we approximate the delta function with Lorentzian function as

$$\delta\,(\omega - x) = \frac{\Gamma}{\pi}\frac{1}{(\omega - x)^2 + \Gamma^2}$$

and set $\Gamma = 1/32$ eV.

We show the calculation results of photoresponsivity coefficient β_{22} as a function of photon energy in Supplementary Fig. 2a. The monotonic behavior against photon energy can be interpreted as follow: In the low energy region (< 2.0 eV), the non-zero coefficient β_{22} is mainly attributed to the transitions near K (K') points, which can be clearly seen in the distribution of β_{22} in momentum space at 1.5 eV (Supplementary Fig. 2b). At higher energies (2.0 eV ~ 2.5 eV), optical transitions around Γ point are allowed, which have the contribution to β_{22} with the opposite sign against those near K (K') points. This cancellation of contributions explains the sharp decrease and increase in the range from 2.0 eV to 2.5 eV. β_{22} reaches its maximum value at 2.5 eV. The momentum space distribution of β_{22} at 2.5 eV (Supplementary Fig. 2c) shows that the transitions near Γ point have a dominant contribution, which explains the origin of the peak around 2.5 eV. As the photon energy is further increased

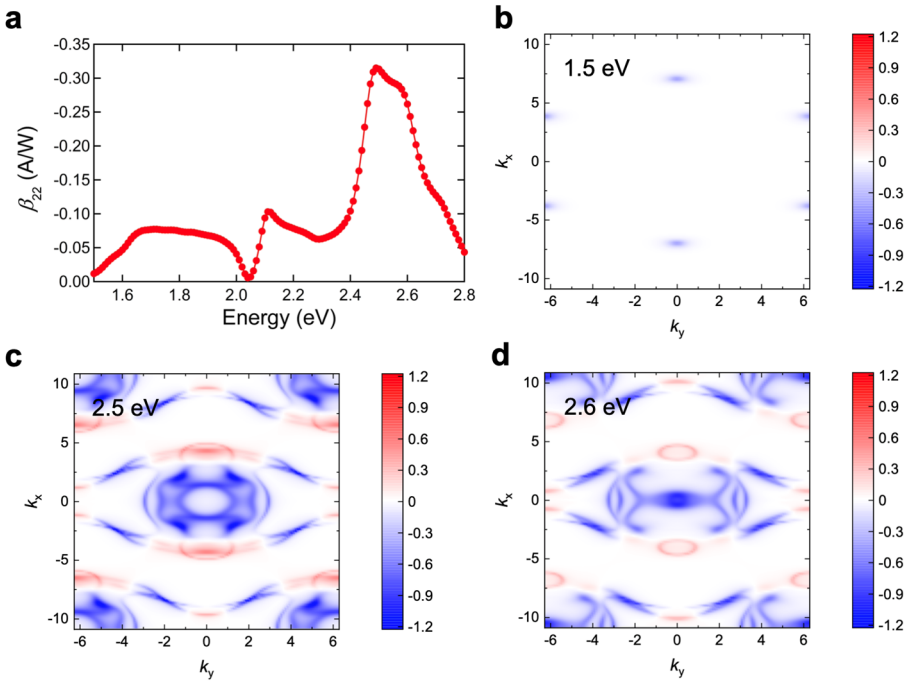

Supplementary Fig. 2| Photon-energy-resolved photoresponsivity coefficient β_{22}. a, Photoresponsivity coefficient β_{22} as a function of photon energy for strained 3R-MoS_2. **b, c, d,** The distribution of photoresponsivity coefficient β_{22} in the momentum space calculated at E = 1.5 eV, 2.5 eV and 2.6 eV, respectively. All the results here are calculated with the parameters ε_x and ε_y set as 1.1 and 0.9.

(> 2.5 eV), more transitions around both K (K') and Γ points are allowed, which contribute to β_{22} with the opposite signs. The photoresponsivity coefficient β_{22} is eventually suppressed due to the cancellation of the signal. In Supplementary Fig. 2d, the momentum space distribution of β_{22} at 2.6 eV confirms the further cancellation at the higher energy region (> 2.5 eV). We note that the exciton effect has not been taken into account, thus the peaks around 1.86 eV and 2.04 eV are not reproduced in the photoresponsivity coefficient spectrum.

We have also calculated the strain dependence of β_{22}, β_{21}, β_{12} and β_{11}, as shown in Supplementary Fig. 3. We set $\varepsilon_x = 1 + e$ and $\varepsilon_y = 1 - e$ in the calculation, and integrate the results over the energy range from 1.5 eV to 2.8 eV. The first conclusion here is that β_{12} and β_{11} are negligibly small, which is consistent with the absence of photocurrent response in zigzag direction of 3R-MoS_2, no matter with or without strain. In the unstrained condition ($\varepsilon_y = 1$), 3R-MoS_2 possesses C_{3v} symmetry, which leads to β_{22} and β_{21} with the same intensity but the opposite signs. By applying a tiny strain (ε_y), a sign change of β_{22} occurs and

then β_{22} and β_{21} have the same sign, reflecting the polar nature under the strain. With the further increase of ε_y, β_{22} monotonously increases at first in a rather linear manner. This quick increase indicates the influence of polarization on the electronic wave functions from the strain. This calculation captures the effect of strain-induced symmetry reduction in 3R-MoS_2. Qualitatively, this calculation result is consistent with the experimental result of strain dependence of photocurrent response in Fig. 4a. However, several details in this calculation are different from the actual experimental results. Firstly, in unstrained 3R-MoS_2, the calculation predicts nonvanishing photocurrent response with a distinct polarization dependence of C_{3v} symmetric systems (a sign change occurs with laser field polarization change), while in experiments we observed extremely small BPVE current ($\sim pA$) from unstrained 3R-MoS_2 samples. This could be understood by the recombination process as explained in the main text. Namely, the recombination process can be more efficient in unstrained samples and may lead to back flow current cancelling the initial shift current response. Secondly, the nonlinear dependence of photocurrent response vs strain is not reproduced by theory, instead, a linear dependence occurs. This difference might result from the simple tight-binding model we considered. Also, suppression of the shift current response in the small strain region from recombination may account for the observed nonlinear behavior. Thirdly, the calculations show an intensity difference between β_{22} and β_{21}, while the experiment does not show much

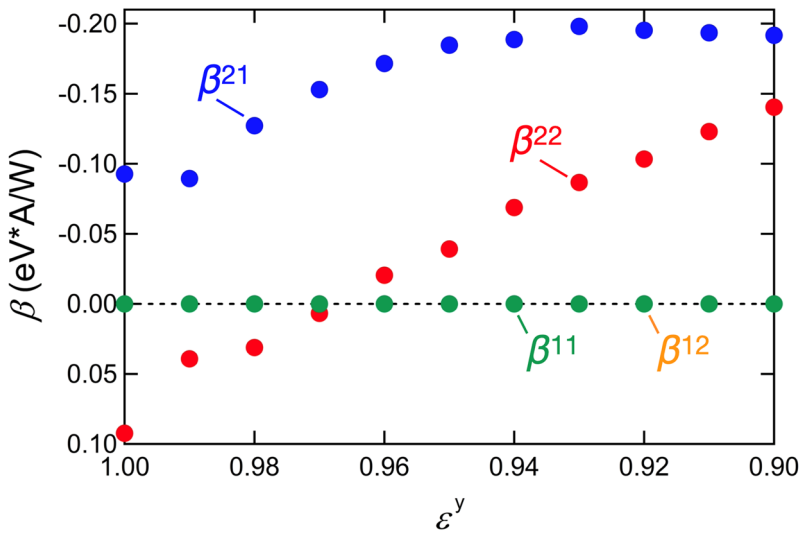

Supplementary Fig.3| Strain dependence of photoresponsivity coefficient κ. Photoresponsivity coefficients β_{22}, β_{21}, β_{12} and β_{11}, (red, blue, orange and green) as a function of strain parameters ε_y, which is taken from 1 to 0.9. The starting state $\varepsilon_y = 1.0$ represents unstrained 3R-MoS_2. This calculation is integrated from 1.5 eV to 2.8 eV.

difference. This discrepancy might also come from the simplicity of our model uniformly modulating the hopping amplitude in the two directions, as more realistic atomic displacements lead to nonuniform hopping modulations.

References

S1. Fang, S., Defo, R. K., Shirodkar, S. N., Lieu, S., Tritsaris, G. A. & Kaxiras, E., *Ab initio tight-binding Hamiltonian for transition metal dichalcogenides*. Phys. Rev. B 92, 205108 (2015).

S2. Cook, A. M., Fregoso, B. M., Juan, F. D., Coh, S. & Moore, J. E., *Design principles for shift current photovoltaics.* Nature Communications. 8, 14176 (2017).

S3. Suzuki, R., Sakano, M., Zhang, Y. J., Akashi, R., Morikawa, D., Harasawa, A., Yaji, K., Kuroda, K., Miyamoto, K. , Okuda, T., Ishizaka, K, Arita, R. & Iwasa, Y., Valley-dependent spin polarization in bulk MoS_2 with broken inversion symmetry. *Nature Nanotechnology* 9, 611-617 (2014).